Journal of ELECTRONIC MATERIALS
https://doi.org/10.1007/s11664-019-07675-9

Intrinsic Magnetic and Ferroelectric Behaviour of Non-magnetic Al^{3+} Ion Substituted Dysprosium Iron Garnet Compounds

M. DHILIP,[1] K. SARAVANA KUMAR,[2] R. RAMESH KUMAR,[3] and V. ANBARASU [4,5]

1.—Department of Physics, SRM Institute of Science and Technology, Ramapuram Campus, Chennai, Tamilnadu 600089, India. 2.—Department of Physics, Sri S. Ramaswamy Naidu Memorial College, Sattur, Tamilnadu 626203, India. 3.—Department of Physics, Anna University, Chennai, Tamilnadu 600025, India. 4.—Department of Physics, PSG College of Arts and Science, Coimbatore, Tamilnadu 641014, India. 5.—e-mail: anbarasu100@gmail.com

Synthetic garnets are a group of oxide materials that play a vital role in the development of solid state lasers, magnetic and optic-electronic devices. The analysis on the solubility of rare-earth elements in the well-crystallized system has led to the discovery of peculiar oxide materials with multifunctional properties. By following the above importance, Aluminium ion (Al^{3+}) substituted Dysprosium Iron Garnet compounds with the chemical formula of $Dy_3Fe_{5-x}Al_xO_{12}$ (x = 0–0.5) have been synthesized by the solid state reaction method and the effect of substitution of non-magnetic ions into the magnetic sub-lattices have been analyzed. The Rietveld refinement of powder x-ray diffraction patterns confirms that the pure $Dy_3Fe_5O_{12}$ compound crystallizes with cubic (Space group: Ia3d) superstructure whereas all the Al^{3+} substituted samples exhibit the coexistence of cubic (*Ia3d*) and trigonal Fe_2O_3 (*R3c*) phases. The energy gap values of the prepared compounds is found to be around 1.6 eV which reveals the semiconducting nature and the decreasing trend of band gap values may be due to the growth factor of crystallites, structural disorder and distortion introduced into the crystal lattice. From the Micro-Raman analysis, it is found that the substituted Al^{3+} ions starts filling into both tetrahedral and octahedral positions and the assignments of vibrational modes observed from Raman spectra confirm the incorporation of Al^{3+} ions into the $Dy_3Fe_5O_{12}$ garnet structure. From the magnetization analysis, it is found that the response of super-exchange interaction between Fe^{3+} ions in the a and d sites of $Dy_3Fe_5O_{12}$ compound leads to net magnetic moment and the substitution of Al^{3+} ions preferably replaces Fe^{3+} ions in d sites and suggests the decrease in net magnetization values. From the photoluminescence studies, it is noticed that the luminescence behavior of Al^{3+} ions substituted $Dy_3Fe_{5-x}Al_xO_{12}$ compounds are due to the superposition of a broad emission band and reveals the variation in concentration of Al^{3+} ions in the prepared compounds. An interesting point to note is that, a well saturated "soft" ferroelectric hysteresis loop is obtained in both pure and Al^{3+} substituted $Dy_3Fe_{5-x}Al_xO_{12}$ compounds, and the observed electric hysteresis loops are found to be influenced by the factors such as capacitance nature, resistivity effects and leakage current of the compounds. Hence, the study on effect of trivalent non-magnetic ion substitution in a hard magnetic $Dy_3Fe_5O_{12}$ system leads to interesting intrinsic magnetic and ferroelectric properties and found suitability for the fabrication of energy storage and optoelectronic devices.

Key words: Rare-earth iron garnet, solid state reaction, Rietveld analysis, Raman spectroscopy, photoluminescence, ferroelectric

(Received March 31, 2019; accepted September 24, 2019)

Published online: 03 October 2019

INTRODUCTION

Dysprosium iron garnet ($Dy_3Fe_5O_{12}$, here after abbreviated as DIG) is a ferrite material with excellent magnetic and optoelectronic properties which makes it as the best material for high-frequency electronic applications.[1] The DIG compound crystallizes in cubic structure (space group Ia3d) in which every unit cell contains eight $R_3^{3+}Fe_5^{3+}O_{12}$ molecules. In the case of ferromagnetic garnet ($R_3Fe_5O_{12}$) structured compounds, the ionic distribution has been represented by $\{R_3\}[Fe_2](Fe_3)O_{12}$, where as the symbols {}, [] () representing 24C {dodecahedral}, 16a [Octahedral], and 24d (tetrahedral) sites, respectively.[2–4] Due to large ionic radius, R^{3+} ions occupy 24c dodecahedral sites and so the Fe^{3+} ions occupy 16a octahedral and 24d tetrahedral sites. It is also to be noted that the substitution of transition metal ions at a Fe-site is a pathway to improve physical properties of DIG compounds and lead to interestingly different phenomena to obtain potential applications.[5–7] $Dy_3Fe_{5-x}Al_xO_{12}$ (hereafter abbreviated as DIAG) belongs to the family of magnetic garnets whose prototype (DIG) is well-known hard (ferro) magnetic materials.[8] In an ideal DIAG, Dy^{3+} ions enter the dodecahedral sites, whereas the iron and aluminium ions occupy tetrahedral and octahedral positions. In specifics, the iron ions preferably occupy octahedral positions and so the smaller aluminium ions fill up the tetrahedral positions.[9,10]

It is found that both the $Dy_3Fe_5O_{12}$ and $Dy_3Al_5O_{12}$ compounds are iso-structural in nature and indicates the possible replacement of ferromagnetic Fe^{3+} ions by diamagnetic Al^{3+} ions.[11,12] It is observed that the substitution of Al^{3+} ions may induce structural distortions followed by metal–insulator transitions and ferromagnetic to paramagnetic behavior. Recently, the diamagnetic dilution of Fe^{3+} sublattices with the rare-earth elements such as Al^{3+}, In^{3+}, Ga^{3+} and Sc^{3+} has received special attention.[13–15] Despite the remarkable utility of magnetic particles in magnetic recording media, permanent magnets and microwave devices, understanding of their magnetic properties still remain unrevealed.[16,17] The role played by substituents on modifying the physical properties of basic garnets and the mechanism of enhancing the magnetic response has been widely studied.

By following the above importance, the effect of non-magnetic Al^{3+} ion substitution on structural, electrical and magnetic properties of Dysprosium Iron Garnet ($Dy_3Fe_5O_{12}$) compound is investigated and the results observed are discussed in the following titles.

EXPERIMENTAL METHOD

Synthesis

Polycrystalline samples of $Dy_3Fe_{5-x}Al_xO_{12}$ (DIAG) (where x = 0.0 [DG], 0.1 [DG1], 0.2 [DG2], 0.3 [DG3], 0.4 [DG4], 0.5 [DG5]) have been prepared by conventional high-temperature solid-state reaction technique under controlled maintenance of time and temperature.[18] Stoichiometric proportions of high purity (99.99%) source compounds such as Dysprosium Oxide (Dy_2O_3—Ants Ceramics), Iron Oxide (Fe_2O_3—Alfa Aesar) and Aluminium Oxide (Al_2O_3—Alfa Aesar) are mixed thoroughly using an agate mortar for a duration of 1 h and sintered at 900°C for 12 h in air atmosphere. The mixture is calcined till 1200°C for 12 h with intermediate grinding. The pre-heated powders are well ground and annealed at 1200°C for 12 h to achieve good crystallinity of the sample. Finally, all the samples are palletized and annealed at 1250°C for 4 h. Then, the obtained samples are used for further characterization.

Characterization

The analyses of crystalline phase formation and structural analysis are carried out using powder x-ray diffraction (XRD) technique. The room temperature powder x-ray diffraction patterns of the prepared compounds are obtained from Bruker AXS D2 phaser x-ray diffractometer using CuKα (1.5418 Å) radiation for the 2θ range of 10°–80° with a step size of 0.02° in the diffractogram. Rietveld refinement for the powder x-ray diffraction data is carried out using the Fullprof suite.[19] The micro-Raman spectral analysis has been carried out using the Renishaw Raman imaging microscope system (Renishaw System 2000), at room temperature. The spectra are collected in the range of 100–1000 cm^{-1}, using a 632 nm He–Ne laser source. The diffused reflectance spectral analysis (DRS) is performed with a Shimadzu UV–Vis–NIR 3600 spectrophotometer incorporated with integrating sphere attachments for the analysis powder samples. The photoluminescence emission and excitation spectra are recorded on a Horiba, (Fluorolog-3) spectrofluorometer at room temperature. The ferroelectric (P–E) behavior of the prepared compounds is analyzed by a P–E loop tracer (Radiant technologies Inc.) with a maximum applied electric field of ~ 10 kV/cm. The magnetization properties are analyzed at room temperature using a Lakeshore 7410 Vibrating Sample Magnetometer with a maximum applied field of 15 kOe.

RESULTS AND DISCUSSION

Structural Properties

The phase stability and structural features of the prepared compounds are analyzed by powder x-ray diffraction technique. The observed powder XRD patterns of $Dy_3Fe_{5-x}Al_xO_{12}$ (x = 0–0.5) samples are analyzed by Rietveld refinement technique and the refined patterns are given in Fig. 1. The calculated lattice cell parameters and reliability factors obtained by Rietveld refinement of $Dy_3Fe_{5-x}Al_xO_{12}$

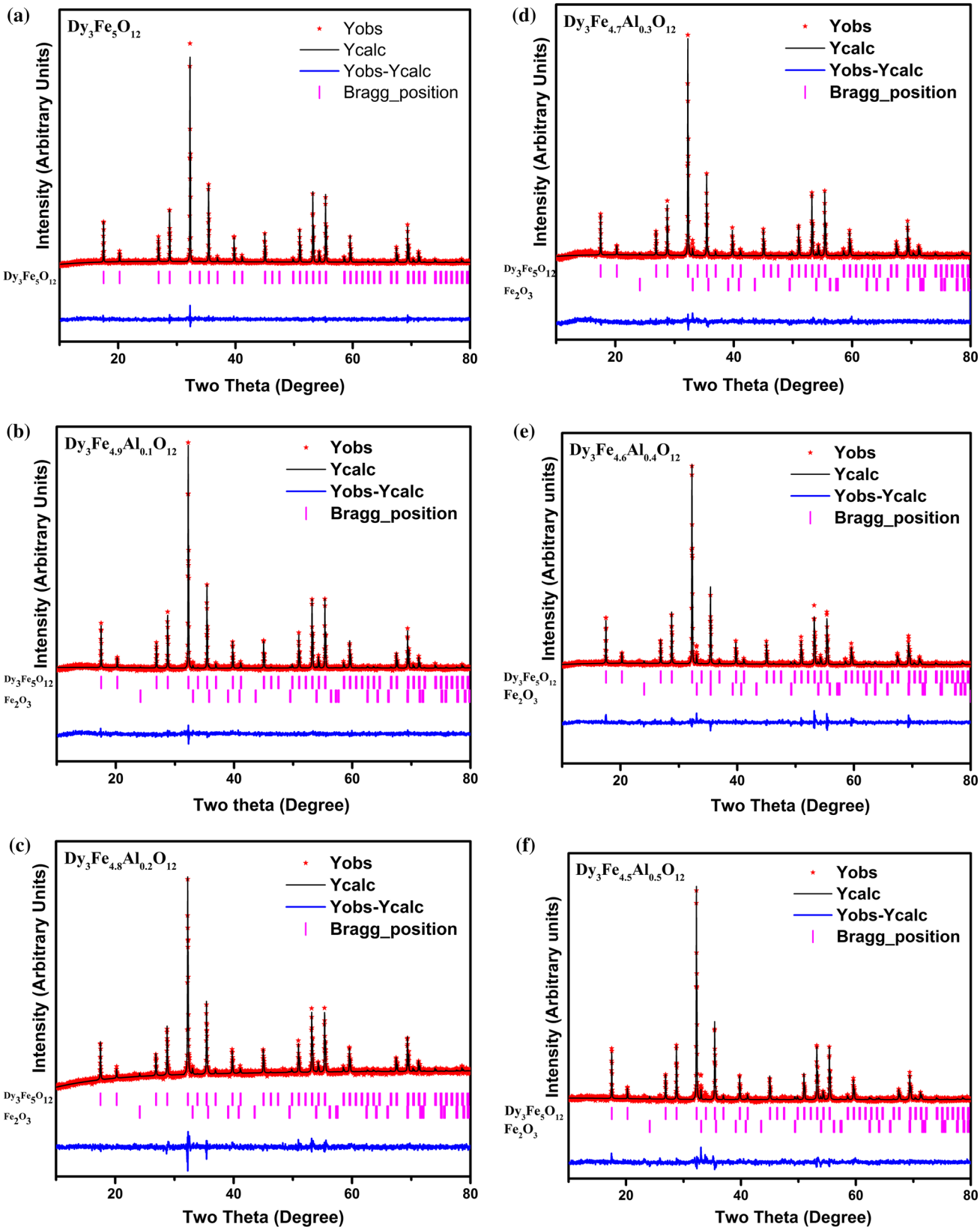

Fig. 1. (a–f) Rietveld refinement patterns of $Dy_3Fe_{5-x}Al_xO_{12}$ (x = 0–0.5) compounds.

Table I. Rietveld refined lattice cell parameters and reliability factors of $Dy_3Fe_{5-x}Al_xO_{12}$ (x = 0–0.5) compounds

	$Dy_3Fe_{5-x}Al_xO_{12}$ system									
	x = 0.0	x = 0.1		x = 0.2		x = 0.3		x = 0.4		x = 0.5	
Rietveld's profile analysis method	Cubic	Cubic	Trigonal	Cubic	Trigonal	Cubic	Trigonal	Cubic	Trigonal	Cubic	Trigonal
Lattice parameters											
a (Å)	12.4095	12.4069	5.0200	12.4086	5.0340	12.4067	5.0313	12.4073	5.0662	12.4040	5.0379
b (Å)	12.4095	12.4069	5.0200	12.4086	5.0340	12.4067	5.0313	12.4073	5.0662	12.4040	5.0379
c (Å)	12.4095	12.4069	13.8638	12.4086	13.8349	12.4067	13.8403	12.4073	13.7817	12.4040	13.8286
Volume (Å^3)	1910.9884	1909.8212	302.5631	1910.5840	303.6229	1909.7001	303.4095	1909.9972	306.3339	1908.9357	303.9479
R factors (%)											
R_p	2.01	2.04	2.04	2.51	2.51	2.32	2.32	2.23	2.23	2.28	2.28
Rwp	2.56	2.57	2.57	3.39	3.39	2.98	2.98	3.09	3.09	3.12	3.12
Rexp	2.27	2.32	2.32	2.59	2.59	2.50	2.50	1.93	1.93	2.23	2.23
X^2	1.27	1.22	1.22	1.71	1.71	1.43	1.43	2.55	2.55	1.96	1.96

(0.0–0.5) compounds are given in Table I. The structural analysis of pure DIG sample reveals the formation of cubic phase with the space group of *Ia3d*. The calculated lattice cell parameters of the DIG sample are found in good agreement with earlier reports related to garnet structure.[20] It is also observed that except pure DIG sample, all the Al^{3+} ion doped samples show coexistence of cubic $Dy_3Fe_5O_{12}$ (*Ia3d*) and trigonal Fe_2O_3 (*R3c*) crystalline phases without any more secondary and/or impurity phases. The formation of Fe_2O_3 phase seems to be unavoidable due to the reaction chemistry of elements. The absence of secondary phases indicates the incorporation of Al into the structure and reveals the dual phase formation. The calculated lattice cell parameters and volume indicate the retention of cubic symmetry with minimum changes in parameters due to incorporation of Al^{3+} ions into the Fe^{3+} ion site of the DIAG system. Due to the substitution of the lower ionic radii Al^{3+} ion (0.53 Å) in the Fe^{3+} ion (0.61 Å) site and larger volume of cubic garnet structure, the incorporation of Al^{3+} ion does not induce any major changes in the lattice cell parameters. Further, it is inferred that there is a possible inducement of the site ordered defects due to the chemical pressure provoked by the incorporation of Al^{3+} ion into the Fe^{3+} site of DIAG compounds. Hence, the structural analysis through the Rietveld refinement process confirms the possible incorporation of non-magnetic Al^{3+} ions into the host $Dy_3Fe_5O_{12}$ garnet structure.

Diffused Reflectance Spectroscopy (DRS) Studies

In order to elucidate the optical response and to determine the band gap of pure and Al^{3+} substituted $Dy_3Fe_5O_{12}$ samples, UV–visible diffused reflectance spectroscopy (UV–Vis DRS) has been utilized. Figure 2 shows the reflectance spectra of pure and Al^{3+} substituted samples for the spectral region of 400–900 nm. From the figure, it is observed that all the samples show optical excitation properties in the visible region and the decreasing trend of reflectivity in the Al^{3+} substituted samples may be due to the presence of distortion in the crystal lattice which is found to be in good agreement with the structural analysis. To calculate the band gap value (E_g) of the prepared samples, the optical reflectance data has been extrapolated by the following equation[21,22]:

$$E_g = \frac{1240}{\lambda}\text{eV},$$

whereas the wavelength (λ) is in nm scale. The calculated band gap values are given in Table II. The observed band gap values (around 1.6 eV) suggests that all the prepared compounds are of semiconducting nature and they are found to be potentially active for high frequency optoelectronic device fabrication. It is also noticed that the band

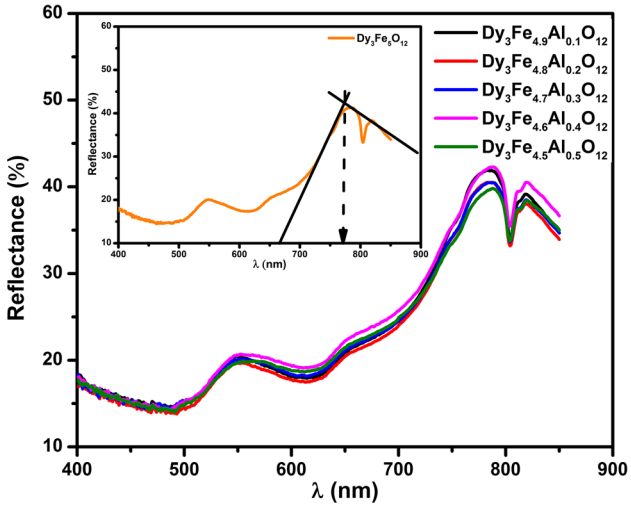

Fig. 2. Diffused reflectance spectra of $Dy_3Fe_{5-x}Al_xO_{12}$ (x = 0–0.5) compounds (inset—$Dy_3Fe_5O_{12}$ compound).

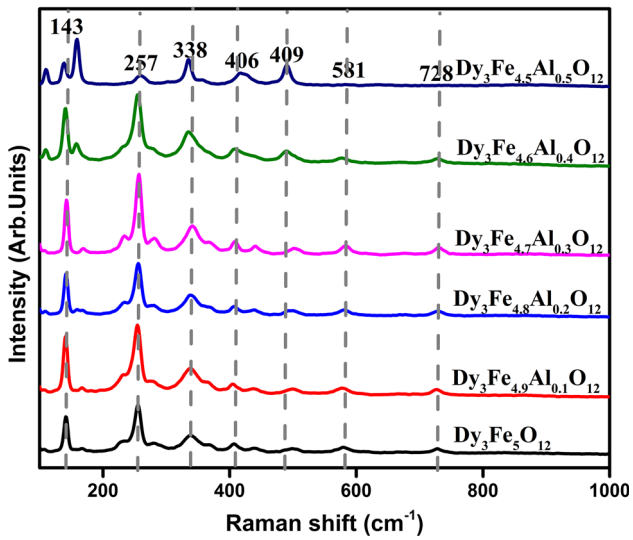

Fig. 3. Normalized Raman spectra of $Dy_3Fe_{5-x}Al_xO_3$ (x = 0–0.5) compounds.

Table II. Energy gap values of $Dy_3Fe_{5-x}Al_xO_{12}$ (x = 0–0.5) compounds

Details of the compound	Cut-off wavelength (nm)	Energy gap (eV)
$Dy_3Fe_3O_{12}$	772	1.606
$Dy_3Fe_{4.9}Al_{0.1}O_{12}$	774	1.602
$Dy_3Fe_{4.8}Al_{0.2}O_{12}$	769	1.612
$Dy_3Fe_{4.7}Al_{0.3}O_{12}$	770	1.610
$Dy_3Fe_{4.6}Al_{0.4}O_{12}$	776	1.597
$Dy_3Fe_{4.5}Al_{0.5}O_{12}$	777	1.595

gap values decrease with respect to the increasing level of Al^{3+} in the $Dy_3Fe_5O_{12}$ compound and the decreasing trend of band gap values may be due to the growth factor of crystallites, structural distortion introduced into the lattice due to breakage of crystal symmetry between a and d site of general garnet structure. Hence, the energy gap analysis refines the variation in site occupancy of Al^{3+} into the DIG garnet structure and confirms the incorporation of Al^{3+} into the DIG garnet structure.

Micro-Raman Analysis

Raman spectroscopy is one of the powerful tools for the analysis of bond length and bond angle between anions and cations in the crystal lattice and structural phase transitions of oxide materials.[23] Raman spectroscopy has the advantage of being very sensitive to structure distortion and oxygen motion and so a detailed investigation of electronic excitation is found to be important for the understanding of garnet structured materials. Hence in the present work, the pure and Al^{3+} ion substituted samples are analyzed by Micro-Raman spectroscopic technique. The normalized Raman spectra of DIG and DIAG samples observed at room temperature are shown in Fig. 3. To improve the analysis, Lorentzian fitting of spectral pattern has been incorporated and given in Fig. 4. From the figure, it is noticed that the Raman spectra show quite obvious variations in the molecular vibrational modes with increasing concentration of substituent (Al) element and this clearly indicates the substitution of Al^{3+}—ion into the tetrahedral and octahedral positions of DIG crystal structure. From the Raman spectra of all the prepared compounds, it is found that the relative intensity of the peak at 728 cm^{-1} is gradually decreased and eventually disappears from the spectrum for the combination of DG5 compound, which is to be explained as follows: As the Al^{3+} ions are substituted into the DIG crystal structure, they gradually fill into Fe^{3+} ion sites in the tetrahedral and octahedral positions. The greater mass of Al^{3+} ion makes the tetrahedrons and octahedrons heavier than before which weakens the vibrational modes and so leads to decrease in relative intensity.[24] As per earlier reports, the resonance peaks arise due to the stretching vibrations between anions and oxygen or between aluminium-centred tetrahedrons or octahedrons and oxygen. The disappearance of vibrational peaks at higher concentrations of Al may be attributed to the replacement of Fe^{3+} ion by the Al^{3+} ion.

The cubic unit cell of a general garnet compound of molecular formula $C_3A_2D_3O_{12}$ contains eight formula units, where C, A, D are metal ions occupying different symmetry sites. The Dy ions (C atom) occupy the 24(c) sites and each Dy^{3+} ion is dodecahedroally coordinated to eight O^{2-} ions. The O^{2-} atoms occupy the 96(h) sites whose exact locations depend on structural parameters (x, y, and z) and are different for different garnet oxides.

In the DIG compound, there are 16 octahedral lattices (with six coordinating oxygen ions) and 24

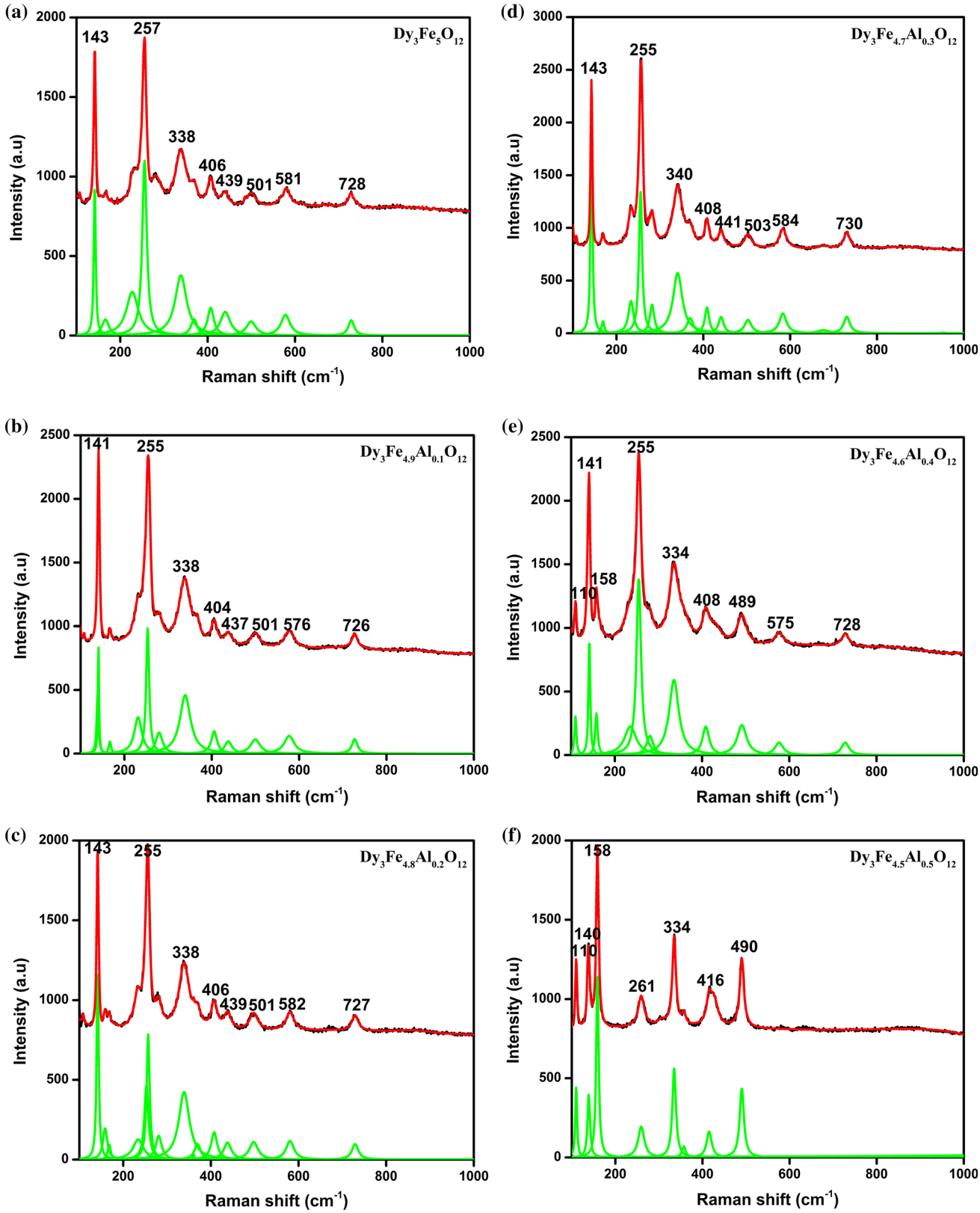

Fig. 4. (a–f) Fitting of Raman signal for the $Dy_3Fe_{5-x}Al_xO_3$ (x = 0.0–0.5) compounds with Lorentzian line shapes. (The black shade is experimental data, the strong curves with green shade are the fitting of Lorentzian shapes and the solid curves with red shade are the total intensities of the Lorentzian lines).

tetrahedral lattices (with four coordinating oxygen ions.[25] The substitution of Al^{3+} ion leads to displacement in either one of these lattices. No more shifts in frequency are observed for the vibrational modes at 257, 338 and 409 cm^{-1}, which reveals that the vibrations are attributed to Dy^{3+} ions. There are only few reports based in rare earth garnet structures, and there is no more study of the lattice dynamical calculations and assignment of Raman modes reported for DIAG materials. The large number of atoms in the primitive cell leads to 240 (3×80) possible modes, which are classified according to the irreducible representation and given by:

$$\Gamma_{\text{total}} = 3A_{1g} + 5A_{2g} + 8E_g + 14F_{1g} + 14F_{2g} + 5A_{1u} + 5A_{2u} + 10E_u + 17F_{1u} + 16F_{2u}.$$

Group theory analysis predicts that 25 modes are Raman active ($3A_{1g}$, $8E_g$ and $14F_{2g}$). A total of 17 modes are IR active (F_{1u} modes; one F_{1u} mode is translational), whereas 55 modes are inactive ($5A_{1u}$, $5A_{2g}$, $16F_{2u}$, $10E_u$, $14F_{1g}$, $5A_{2u}$) as similar to the Yttrium Iron Garnet (YIG) system.[26] Out of 25 Raman active vibrational modes, 9 vibrational modes have been observed in the spectral region of 100–1000 cm^{-1}. For the iron garnet materials, the Raman active modes correspond to internal modes, translational and rotational modes, respectively. Raman active modes below 200 cm^{-1} are contributed by translation of Fe^{3+} (16a), Dy^{3+} (24c) and Fe^{2+} (24d) sites. From the figure, it is found that the internal modes of vibrations are present at the frequency of about 338, 501, 581 and 728 cm^{-1} respectively. Because of the variation in concentration of Al^{3+} ion, there is a slight variation in resonance modes that are also observed. Assignments of all the vibrational modes observed from Raman's spectra are described in Table III and the matching of vibrational modes of pure and Al^{3+} ions substituted compounds confirm the incorporation of Al^{3+} ions into the DIG host lattice.

Table III. Assignment of Raman modes of $Dy_3Fe_{5-x}Al_xO_{12}$ (x = 0–0.5) compounds

Detail of the compound and symmetry assignments							Vibrational mode
$Dy_3Fe_5O_{12}$	$Dy_3Fe_{4.9}Al_{0.1}O_{12}$	$Dy_3Fe_{4.8}Al_{0.2}O_{12}$	$Dy_3Fe_{4.7}Al_{0.3}O_{12}$	$Dy_3Fe_{4.6}Al_{0.4}O_{12}$	$Dy_3Fe_{4.5}Al_{0.5}O_{12}$		
143	141	143	143	110 141	110 140		Fg Fg
				158	158		Fg
257	255	255	255	255	261		Ag
338	338	338	340	334	334		Fg + Ag
406	404	406	408	408			Fg + Eg
					416		Fg
439	437	439	441				Fg + Ag
				489	490		Fg + Ag
501	501	501	503				Fg + Ag
581	576	582	584	575			Fg + Ag
728	726	727	730	728			Fg + Eg

Magnetization Analysis

In order to understand the effect of non-magnetic Al^{3+} ion substitution in magnetic properties of DIG compounds, magnetization measurements are taken using a vibrating sample magnetometer at room temperature with a maximum applied field of 15 kOe, and it is found that the magnetization values monotonically increased with applied field, as shown in Fig. 5. In the DIG compound, the Dy^{3+}(c site) site is eight-fold dodecahedrally coordinated where as the Fe^{3+} (a site) site is of six-fold octahedra and the Fe^{3+} (d site) site is four-fold tetrahedrally coordinated. As the Dy^{3+} ion is paramagnetic, the resultant magnetic moment arises from the super-exchange interactions between the Fe^{3+} ions in a and d sites. As per earlier reports, the a-d interactions are dominant while comparing to a–a and d–d interactions.[27] Hence, the resultant magnetic

moment is the response of super-exchange interaction between Fe^{3+} in a and d sites. According to present case, Al^{3+} ions preferably substitutes Fe^{3+} ions in d sites in minimum quantities and tends to substitute octahedral sites while increasing the concentration Al^{3+} ions. Since Fe^{3+} ions are replaced by the non-magnetic Al^{3+} ions in d and a sites, the super-exchange interactions of Fe^{3+} ions are modified extensively and reveals the decrease in net magnetization values.[28–30] From the hysteresis loops, the coercive field (H_C), saturation magnetization (M_S) and ratio of remanence to saturation magnetization (M_R/M_S) have been calculated and listed in Table IV. With the increase in Al^{3+} content, saturation magnetization (M_S) decreases from the value of 6.4–4.6 emu/g and these results confirm the substitution of ferromagnetic Fe^{3+} ions with diamagnetic Al^{3+} ions. From the earlier reports, it is found that during substitution, Al^{3+} ions prefer to accommodate in tetrahedral sites with lower ionic radii.[31] In the present case of pure Dysprosium Iron Garnet, the decrease in M_S has been attributed to the surface effect, which may be linked with disorder or non-alignment of surface spins. The non-magnetic Al^{3+} ions having no net magnetic moment replaces Fe^{3+} ions ($5\mu_B$) from the sites having favorable conditions for ferromagnetic alignment, thereby reducing the saturation. The net magnetic moments in the ferromagnetic garnet materials depend on the number of magnetic ions occupying the tetrahedral and octahedral sites. Therefore, the change in the magnetization behavior depends on number and type of magnetic ions at a-and d-sites.[32] In a DIG system, the magnetic moment of two Fe^{3+} ions in a-site is aligned antiparallel to that of three Fe^{3+} in the d-site.[33,34] Therefore, the saturation magnetization of DIG is induced due to the magnetic Fe^{3+} ions in the d-sites and the net magnetic moment is calculated as:

$$\begin{aligned} M(\mathrm{DIG}) &= |M_d - M_a| - (-M_c) \\ &= \left|3M_{\mathrm{Fe}}^{3+} - 2M_{\mathrm{Fe}}^{3+}\right| . \\ &= 5\mu_B (Mc \neq 0) \end{aligned}$$

The variation of saturation magnetization (M_s) with respect to increasing concentration of Al^{3+} ion is shown in Fig. 6, which reveals the decreasing trend of magnetization behavior. Since, Fe^{3+} ions in d-site or a-site is substituted by Al^{3+} ion, the ion distribution can be represented as:

$$\{Dy_3\}\left[\mathrm{Fe}_{2-y}\mathrm{Al}_y\right](\mathrm{Fe}_{3-z}\mathrm{Al}_z)\mathrm{O}_{12}.$$

The value of magnetic moment of Al^{3+} ion is much smaller than that of Fe^{3+} ion and if Al^{3+} ions enter the d-site completely (z = 0), then the total saturation will increase. The argument is true for vice versa, when y = 0. Although the radius of Al^{3+} ion is smaller than the radius of Fe^{3+} (which occupy both a- and d-sites), the octahedral a-site is preferable. The reason being the octahedral site is surrounded by six oxygen ions, and Al^{3+} is more stable at the octahedral site than the tetrahedral site. Here the net magnetic moment is as follows:

$$\begin{aligned} M &= |Md - Ma| \\ &\quad - (-Mc)\left(\mu_{\mathrm{Al}}^{3+} = 0\mu_B,\ \mu_{\mathrm{Fe}}^{3+} = 5\mu_B,\ \mu_{\mathrm{Al}}^{3+} \ll \mu_{\mathrm{Fe}}^{3+}\right). \end{aligned}$$

From the Fig. 6, it is observed that the net magnetization decreases with increasing concentration of Al^{3+} ions and indicates that Al^{3+} ions have been incorporated into the tetrahedral (d) site as well as the octahedral (a) site.

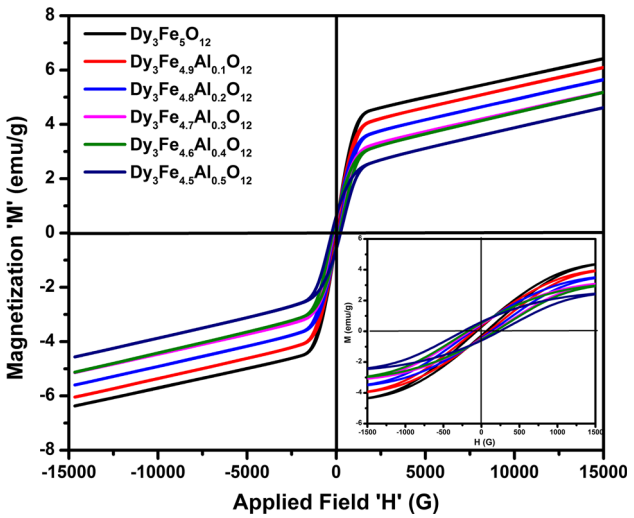

Fig. 5. Magnetic hysteresis loop of $Dy_3Fe_{5-x}Al_xO_3$ (x = 0–0.5) compounds (inset—enlarged view of hysteresis curve).

Table IV. Magnetization properties of $Dy_3Fe_{5-x}Al_xO_{12}$ (x = 0–0.5) compounds

Sample details	Magnetic saturation (M_S) (emu/g)	Magnetic retentivity (M_R) emu/g	Coercivity (H_c) Gauss	Squareness ratio (M_R/M_S)
$Dy_3Fe_5O_{12}$	6.4196	0.4121	86.997	0.0641
$Dy_3Fe_{4.9}Al_{0.1}O_{12}$	6.0938	0.5379	121.87	0.0882
$Dy_3Fe_{4.8}Al_{0.2}O_{12}$	5.6492	0.6630	162.86	0.1173
$Dy_3Fe_{4.7}Al_{0.3}O_{12}$	5.1908	0.7291	195.94	0.1404
$Dy_3Fe_{4.6}Al_{0.4}O_{12}$	5.1796	0.8067	219.33	0.1557
$Dy_3Fe_{4.5}Al_{0.5}O_{12}$	4.6157	0.8960	277.49	0.1941

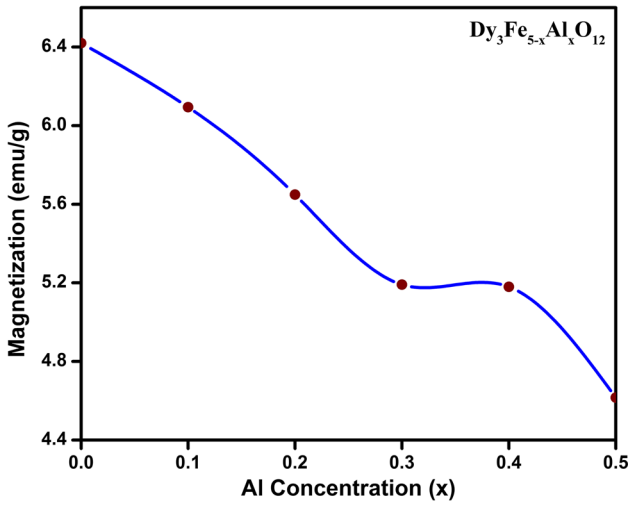

Fig. 6. Magnetic saturation of $Dy_3Fe_{5-x}Al_xO_3$ (x = 0–0.5) compounds as a function of x.

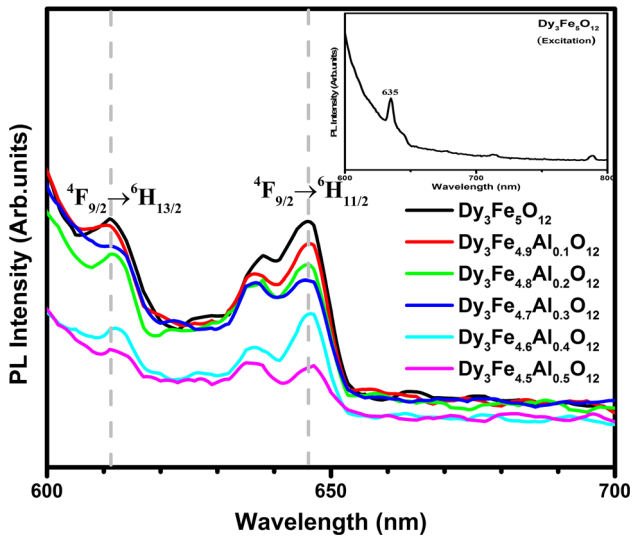

Fig. 7. Photoluminescence emission spectra of $Dy_3Fe_{5-x}Al_xO_3$ (x = 0.0–0.5) compounds.

From the Table IV, it is found that the coercivity (H_C) of the samples increases from 86.9 G for DG to its highest value of 277.5 G for DG5. Remanent magnetization (M_R) values is also found to be increasing with respect to the increasing concentration of Al^{3+} ion (in the range of 0.4121–0.8960 emu/g). The coercivity and remanent magnetization mechanism depend on intrinsic and extrinsic properties of the material. Intrinsic properties depend on crystal structure and chemical composition. The extrinsic properties are dependent upon the microstructure of the bulk material such as defects, grain size and grain shape. Hence, the gradual increase in coercive field and remanent magnetization confirms the incorporation of Al^{3+} ions into the crystal lattice of $Dy_3Fe_5O_{12}$ compound and reveals the possible substituent induced structural disorder in the prepared compounds.

Photoluminescence Studies

Figure 7 shows the room temperature photoluminescence spectra of pure and Al^{3+} substituted samples, excited at 635 nm (Inset Fig. 7) and details of emission spectra are listed in Table V. The PL spectra exhibit two major groups of emission lines. The yellow and red emissions are assigned to ($^4F_{9/2} \rightarrow {}^6H_{13/2}$) and ($^4F_{9/2} \rightarrow {}^6H_{11/2}$) transactions, respectively.[35] Further, it is to be noted that in the case of DIG, the integrated intensity of yellow emission is greater than that of red emission. It is well known that the yellow ($^4F_{9/2} \rightarrow {}^6H_{13/2}$) emission of Dy^{3+} ions belongs to the hypersensitive (forced electric dipole) transition with the selection rule of $\Delta J = 2$, which is strongly influenced the by surrounding environment and is well correlated with the Kramer's doublets $(2J + 1)/2$, where J is the total angular momentum of the electrons.[36–38] It is also noticed that the fluorescence intensity decreases with increasing concentration of Al^{3+} ions. At higher concentration, the reduction in PL emission intensity is due to the factor of quenching.[39] As the concentration increases, the distance between the activator ions becomes less, which leads to higher probability of energy transfer between these ions.

The concentration of quenching mainly arises because of non-radiative energy transfer between the activator ions and generally described by the methods such as exchange interactions, radiation re-absorption, or the multipolar interactions.[40] The type of interaction mechanism can be identified by knowing the critical distance between the adjacent activator ions. Generally non-radiative energy transfer plays an important role in quenching of emission intensities. Due to small energy gaps between all the states lying above 6000 cm^{-1}, the $^4F_{9/2}$ state is rapidly populated by non-radiative relaxation. Then, quite strong yellow and red luminescence originating from $^4F_{9/2}$ state is observed. This case has been represented by the energy level diagram of emissions and other processes such as non-radiative energy transfer as shown in Fig. 8. The $^4F_{9/2}$ level possesses purely radiative relaxation, since this level has sufficient energy gap ($\sim$ 4000 cm^{-1}) with respect to the next lower level ($^6F_{1/2}$). In order to study the effect of Al^{3+} concentration on the luminescence intensity, the photoluminescence has been measured for the whole series of samples. In the present case, the red emission dominates the yellow emission and specifies the symmetric nature of the host lattice. As the luminescence of the substituted system is due to superposition of host, broad emission band extending from 600 nm to 700 nm reveals the variation in composition of Al^{3+} ions in the prepared compounds. The emission band in the visible region is composed of many peaks merged into a broad band and the

Table V. Details of emission spectra of $Dy_3Fe_{5-x}Al_xO_{12}$ (x = 0–0.5) compounds

Wavelength (nm)	Energy (eV)	Wavenumber (cm^{-1})	Transition
612	2.02	16339	$^4F_{9/2} \rightarrow {}^6H_{13/2}$
645	1.92	15504	$^4F_{9/2} \rightarrow {}^6H_{11/2}$

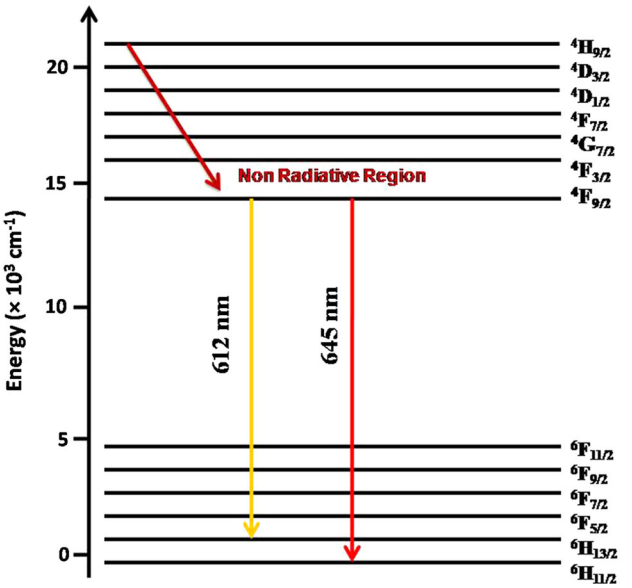

Fig. 8. Energy level diagram and emission transitions of $Dy_3Fe_{5-x}Al_xO_3$ (x = 0.0–0.5) compounds.

broad band has been attributed due to defects such as oxygen vacancies, oxygen interstitial and oxygen antisites. The defects could generate an energy gap between the valence band and the conduction band which results with decreasing trend of energy gap (E_g) values of DIAG compounds as observed from diffused reflectance studies.

Electric Polarization Analysis

The electric polarization nature of all the samples are measured by *P–E* loop tracer at room temperature and given in Fig. 9. The variation in remanent polarization (P_r), saturated polarization (P_s) and coercive field (E_c) with respect to the applied electric field are listed in Table VI. From the figure, saturated "soft" *P–E* Loops with a remanent polarization (P_r) of 0.67 μC cm^{-2} and coercivity (E_c) of 2.05 kV cm^{-1} is obtained for the pure $Dy_3Fe_5O_{12}$ compound. It is also evident that the electric polarization properties of DIAG compounds are strongly affected due to the substitution of Al^{3+} ions into the $Dy_3Fe_5O_{12}$ compounds. It is also noted that the remanent polarization (P_r) and the saturated polarization (P_s) values are found to be increasing with respect to increasing concentration of Al^{3+} ion

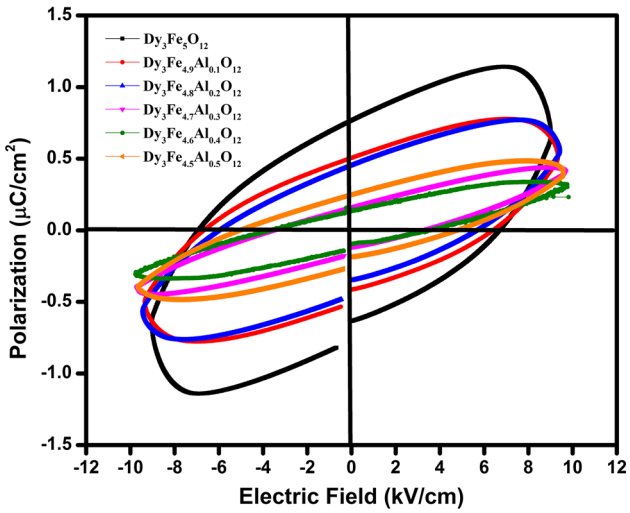

Fig. 9. Electric polarization nature of $Dy_3Fe_{5-x}Al_xO_3$ (x = 0.0–0.5) compounds.

Table VI. Details of saturation polarization (P_s), Remanent polarization (P_R), electric field (E_c) of $Dy_3Fe_{5-x}Al_xO_{12}$ (x = 0.0–0.5) compounds

Sample details	Saturation polarization (P_S) ($\mu C/cm^2$)	Remanent polarization (P_R) ($\mu C/cm^2$)	Electric field (E_c) (kV/cm)
$Dy_3Fe_5O_{12}$	1.15	0.67	2.05
$Dy_3Fe_{4.9}Al_{0.1}O_{12}$	0.79	0.51	2.31
$Dy_3Fe_{4.8}Al_{0.2}O_{12}$	0.80	0.56	2.38
$Dy_3Fe_{4.7}Al_{0.3}O_{12}$	0.45	0.40	1.26
$Dy_3Fe_{4.6}Al_{0.4}O_{12}$	0.35	0.23	1.36
$Dy_3Fe_{4.5}Al_{0.5}O_{12}$	0.50	0.40	2.09

and then decreases, whereas the coercive field (E_C) decreases continuously. It is worth nothing that the samples exhibit typical rectangle hysteresis loops. However, for the maximum substitution level of Al^{3+} ion (x = 0.5), the hysteresis loop becomes pinched and slimmed. Here, the shape of the polarization curve could be related to conductivity rather than electrical polarization. It should be noted that the *P–E* loops could not attain the complete saturation and be strongly influenced by resistive losses. Hence, the electric hysteresis loop of $Dy_3Fe_{5-x}Al_xO_{12}$ (x = 0–0.5) compounds have been found to be influenced by the capacitive nature, resistivity effects and leakage current of the compounds as well, and the values obtained are quite comparable with earlier reports related to garnet structure.[41,42]

CONCLUSION

The effect of non-magnetic (Al^{3+}) ion substitution into the garnet structured $Dy_3Fe_5O_{12}$ compound has been analyzed by Rietveld refinement of powder x-ray diffraction patterns and confirms the

formation of a single phase and reveals the cubic (Ia3d) structure of the DIG compound and the coexistence of both cubic (Ia3d) and trigonal (R3c) symmetry in DIAG compounds. The decreasing trend of the band gap values make explicit the possibility of induced structural disorder and distortion in the crystal lattice due to breakage of symmetry between a and d site Fe^{3+} ions in DIG cubic structure. The Raman scattering measurement reveals a prominent vibrational band around 100–1000 cm^{-1} for all the prepared compounds. The variation in prominent frequency shift, line broadening and intensity are noticed with respect to the increasing concentration of Al^{3+} ions into the DIG and suggests the structural transformation as revealed by structural refinement from powder x-ray diffraction patterns. The magnetic hysteresis behavior of pure and Al substituted samples are characterized by their moderate magnetization nature, and the decreasing trend in net magnetization indicates that Al^{3+} ions have been incorporated into the tetrahedral (d) site as well as octahedral (a) site and subsidize the suppression of magnetic moments while increasing concentration of Al^{3+} ions. The photoluminescence emission spectra show two strong emission bands in yellow ($^4F_{9/2} \rightarrow {}^6H_{13/2}$) and Red ($^4F_{9/2} \rightarrow {}^6H_{11/2}$) regions. The emission band in the visible region has been composed by many peaks and merged into a broad band which is attributed due to defects such as oxygen vacancies, oxygen interstitial and oxygen antisites. As a consequence of effect of sintering temperature and substitution of non-magnetic elements, a saturated P–E loop is observed for the pure $Dy_3Fe_5O_{12}$ compound whereas all other Al^{3+} ion substituted compounds show soft electric polarization curves and confirm the possibility of tuning the polarization behavior via substitution of non-magnetic ions into the ferromagnetic garnet materials. Therefore, the effective replacement of magnetic ions with non-magnetic lattices leads to modification of physical properties and signifies their utility as multifunctional materials. The fascinating electric and magnetic polarization properties of the prepared samples reveal the suitability for the applications in the field of opto-electronics and magneto-optic devices.

REFERENCES

1. M.N. Akhtar, M. Yousaf, S.N. Khan, M.S. Nazir, M. Ahmad, and M.A. Khan, *Ceram. Int.* 43, 17032 (2017).
2. Y. Kohara, Y. Yamasaki, Y. Onose, and Y. Tokura, *Phys. Rev. B Condens. Matter Mater. Phys.* 82, 1 (2010).
3. J. Su, X. Lu, C. Zhang, J. Zhang, H. Sun, C. Ju, Z. Wang, K. Min, F. Huang, and J. Zhu, *Phys. B Condens. Matter* 407, 485 (2012).
4. P. Manimuthu and C. Venkateswaran, *Mater. Lett.* 155, 8 (2015).
5. W. Wang, R. Chen, and K. Wang, *IEEE Trans. Magn.* 48, 3638 (2012).
6. R. Fujikawa, A.V. Baryshev, J. Kim, H. Uchida, and M. Inoue, *J. Appl. Phys.* 103, 07D301 (2008).
7. R. Tholkappiyan and K. Vishista, *Appl. Surf. Sci.* 351, 1016 (2015).
8. C. Suchomski, C. Reitz, C.T. Sousa, J.P. Araujo, and T. Brezesinski, *Chem. Mater.* 25, 2527 (2013).
9. D. Rodic, M. Mitric, R. Tellgren, and H. Rundlof, *J. Magn. Magn. Mater.* 232, 1 (2001).
10. S. Thongmee, P. Winotai, and I.M. Tang, *Solid State Commun.* 109, 471 (1999).
11. Z.A. Motlagh, M. Mozaffari, J. Amighian, A.F. Lehlooh, M. Awawdeh, and S. Mahmood, *Hyperfine Interact.* 198, 295 (2010).
12. K. Sadhana, S. Ramana Murthy, and K. Praveena, *Mater. Sci. Semicond. Process.* 34, 305 (2015).
13. M. Pardavi-Horvath, *J. Magn. Magn. Mater.* 215, 171 (2000).
14. G.F. Dionne, *Magnetic Oxides* (Berlin: Springer, 2009), pp. 107–150.
15. T.Y. Kim and Y. Yamazaki, *IEEE Trans. Magn.* 40, 2793 (2004).
16. M.A. Musa, R.S. Azis, N.H. Osman, J. Hassan, and M.M. Dihom, *J. Aust. Ceram. Soc.* 54, 55 (2018).
17. V.G. Harris, A. Geiler, Y. Chen, S.D. Yoon, M. Wu, A. Yang, Z. Chen, P. He, P.V. Parimi, X. Zuo, C.E. Patton, M. Abe, O. Acher, and C. Vittoria, *J. Magn. Magn. Mater.* 321, 2035 (2009).
18. V. Anbarasu, M. Dhilip, K. Saravana Kumar, and K. Sivakumar, *J. Mater. Sci.: Mater. Electron.* 28, 8976 (2017).
19. H.M. Rietveld, *J. Appl. Crystallogr.* 2, 65 (1969).
20. M. Guillot, C.N. Chinnasamy, J.M. Greneche, and V.G. Harris, *J. Appl. Phys.* 111, 10 (2012).
21. A. Manigandan, V. Anbarasu, B. Sathyaseelan, and K. Sivakumar, *Int. J. Mod. Phys. B* 28, 1450156 (2014).
22. Y. Zheng, W. Zhuang, X. Xing, J. Zhong, R. Liu, Y. Li, Y. Liu, and Y. Hu, *RSC Adv.* 6, 68852 (2016).
23. V. Srinu Bhadram, B. Rajeswaran, A. Sundaresan, and C. Narayana, *EPL* 101, 17008 (2013).
24. P. Ortega, M. Ramirez, C. Foschini, F. Garcia, M. Cilense, and A. Simoes, *Process. Appl. Ceram.* 8, 211 (2014).
25. M.S. Lataifeh, *Appl. Phys. A Mater. Sci. Process.* 92, 681 (2008).
26. D.M. Hemeda, A. Tawfik, O.M. Hemeda, and S.M. Dewidar, *Solid State Sci.* 11, 1350 (2009).
27. L.S. Xie, G.X. Jin, L. He, G.E.W. Bauer, J. Barker, and K. Xia, *Phys. Rev. B* 95, 1 (2017).
28. M.S. Lataifeh, *J. Phys. Soc. Jpn.* 69, 2280 (2000).
29. Y.F. Chen, K.T. Wu, Y.D. Yao, C.H. Peng, K.L. You, and W.S. Tse, *Microelectron. Eng.* 81, 329 (2005).
30. C.S. Kim, B.K. Min, S.J. Kim, S.R. Yoon, and Y.R. Uhm, *J. Magn. Magn. Mater.* 254–255, 553 (2003).
31. J. Ostorero and M. Guillot, *J. Appl. Phys.* 91, 7296 (2002).
32. Z. Cheng, H. Yang, Y. Cui, L. Yu, X. Zhao, and S. Feng, *J. Magn. Magn. Mater.* 308, 5 (2007).
33. W. Wang, R. Chen, and X. Qi, *J. Alloys Compd.* 512, 128 (2012).
34. W. Wang, X. Zhao, J. Zhuang, Y. Zhang, W. Guo, and M. Lahoubi, *J. Magn. Magn. Mater.* 360, 193 (2014).
35. C. Madhukar Reddy, G. R. Dillip, K. Mallikarjuna, B. Sudhakar Reddy, K. Vemasevana Raju, and B. Deva Prasad Raju, *Photonics Lett. Pol.* **3**, 32 (2011).
36. J. Mulak and M. Mulak, *J. Phys. A: Math. Theor.* 40, 2063 (2007).
37. J.B. Gruber, B. Zandi, U.V. Valiev, and S.A. Rakhimov, *J. Appl. Phys.* 94, 1030 (2003).
38. M.D. Chambers and D.R. Clarke, *Annu. Rev. Mater. Res.* 39, 325 (2009).
39. H.W. Leverenz and F. Seitz, *J. Appl. Phys.* 10, 479 (1939).
40. X. Zhang, F. Zhou, J. Shi, and M. Gong, *Mater. Lett.* 63, 852 (2009).
41. J. Su, Y. Guo, J. Zhang, H. Sun, J. He, X. Lu, C. Lu, and J. Zhu, *Ferroelectrics* 448, 71 (2013).
42. A. Duran, C. Ostos, O. Arnache, J.M. Siqueiros, and M. Garcia-Guaderrama, *J. Appl. Phys.* 122, 134101 (2017).